ARMY RESEARCH LABORATORY

Thermal Analysis of a Subminiature Telemetry Sensor Mounted in a Kinetic Energy Projectile Base

Michael S.L. Hollis
Bernard J. Guidos
Paul J. Conroy

ARL-TR-1425   AUGUST 1997

19971010 055

DTIC QUALITY INSPECTED 3

Army Research Laboratory

Aberdeen Proving Ground, MD 21005-5066

Thermal Analysis of a Subminiature Telemetry Sensor Mounted in a Kinetic Energy Projectile Base

Michael S.L. Hollis
Bernard J. Guidos
Paul J. Conroy
Weapons and Materials Research Directorate

DTIC QUALITY INSPECTED 8

Abstract

A computational thermal analysis is presented for a hardened subminiature telemetry sensor system (HSTSS) mounted in the tracer well of a large caliber fin-stabilized kinetic energy projectile. The HSTSS discussed here is designed to provide a record of roll history. The in-bore and in-flight projectile surface heat transfer conditions are adapted from two previous studies in numerical interior ballistic and computational aerodynamics. The combined heat transfer model is used in the present study to provide boundary conditions for computations of surface and in-depth transient thermal response of the HSTSS components. A two-dimensional axisymmetric multiple material numerical approach is used to model the HSTSS and projectile base over the complete in-bore and in-flight event. A one-dimensional numerical approach with a surface melt condition is used to model the protective plastic radome on the HSTSS while in bore. A one-dimensional analytical approach for high-speed melting is presented and compared to the numerical model. The analysis allows a pre-test evaluation to be made of the thermal integrity of the HSTSS design for a large caliber launch and flight environment.

TABLE OF CONTENTS

INTENTIONALLY LEFT BLANK

LIST OF FIGURES

INTENTIONALLY LEFT BLANK

LIST OF TABLES

INTENTIONALLY LEFT BLANK

1. INTRODUCTION

The Hardened Subminiature Telemetry and Sensor System (HSTSS) program within the U.S. Army is centering on the identification and demonstration of new technologies to support gun-launched munition test measurements (D'Amico, Burke, Faulstich, & Hooper 1996). One area of focus is the development of an HSTSS instrumentation package to mount in the base of a conventional large caliber fin-stabilized kinetic energy (KE) projectile. The HSTSS may be designed to provide on-board measurements of projectile attitude, accelaration, or internal diagnostics such as pressure and temperature. The data will be telemetered to a ground station while the projectile is in flight, providing direct real-time data critical to the development of new munitions, particularly smart munitions.

A new generation of rugged subminiature components has been a focus of study (Burdeshaw & Clay 1991; Davis 1996a, 1996b). The on-board HSTSS instrumentation must survive the hostile launch and flight environments associated with large caliber weapons systems. The present study addresses the thermal viability of a current HSTSS design subjected to the in-bore and in-flight heating of such a system. Numerical simulations of interior ballistics, aerodynamics, and transient heat conduction are combined to predict the thermal response of the HSTSS components. The objectives are to (1) make a pre-flight prediction of the in-bore and in-flight thermal integrity of the HSTSS design and (2) identify HSTSS components most likely to be sources of thermal failure, should it occur.

The in-bore and in-flight projectile surface heat transfer conditions are adapted from two separate studies in numerical interior ballistics and computational aerodynamics. The resulting combined heat transfer model is used in the present study to provide boundary conditions for computations of surface and in-depth transient thermal response of the HSTSS components. A two-dimensional (2-D) axisymmetric multiple material numerical approach is used to simulate the thermal response in the HSTSS over the complete in-bore and in-flight event. A one-dimensional (1-D) numerical approach with a surface melt condition is used to simulate the thermal response and surface regression of the protective radome on the HSTSS while in bore. A 1-D analytical model for high-speed melting is presented and compared to the 1-D numerical model. Thermal survivability criteria appropriate for the HSTSS components are compiled and applied to the numerical results to characterize the thermal viability of the current design.

2. PROJECTILE AND HSTSS CONFIGURATIONS

A candidate projectile for testing the HSTSS is a 120-mm configuration known as the Hollow Aluminum Training Round (HATR), shown in Figure 1. Typical of long rod KE configurations, the HATR is a fin-stabilized, discarding sabot design. The HATR projectile possesses a conical nose section followed by a cylindrical section of constant diameter 37.4 mm (1 caliber). The total length is 13 calibers, with sabot grooves covering much of the cylindrical portion. The projectile configuration consists mostly of aluminum and weighs approximately 0.91 kg, rendering it much lighter than fielded 120-mm projectiles and with a significantly reduced maximum range. The HATR is designed as a ballistic match for the M865 training round. Unpublished Weibel radar data from HATR test firings show the HATR to have roughly the same velocity history as the M865. The M865 velocity at the muzzle and at 3-km range are given by Department of the Army Firing Table FT-120-D-1 as 1700 m/s and 677 m/s, respectively, and the flight time is given as 2.7 seconds. The in-bore time of the HATR is assumed to be 5.5 ms, compared to 7 ms for the M865.
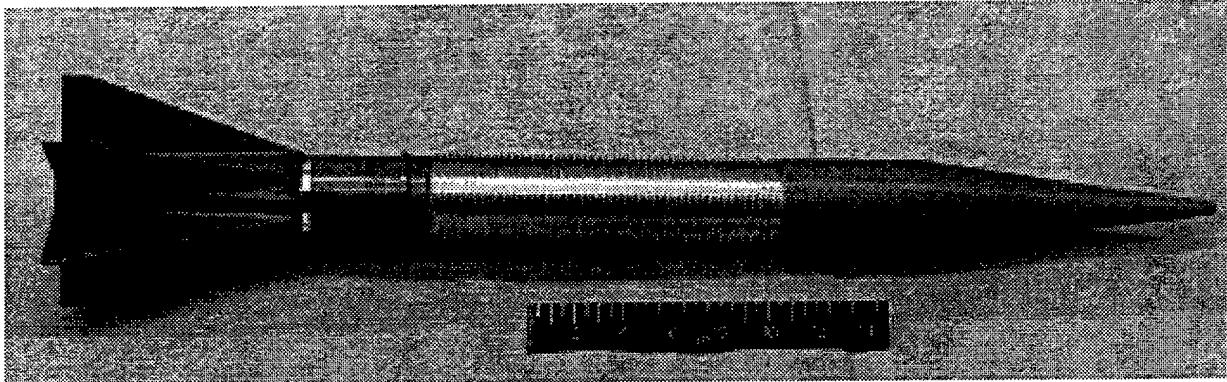
Figure 1. HATR Projectile.

The six-fin hub is an off-the-shelf component taken from the M735 projectile and is composed of aluminum with an annodized aluminum oxide protective coating. A threaded tracer well is located in the fin hub base. A tracer is used in both testing and actual engagement to aid in the visual spotting of the fired round. For HSTSS applications, the tracer is replaced by the instrumentation package. The tracer well is centered on the projectile axis and is approximately 21 mm in diameter and 25.7 mm in depth.

The present HSTSS design provides a measurement of roll history, and the major components are illustrated in Figure 2. One of the two circuit boards contains a g-switch, transmitter, amplifier, and voltage regulator; the other is a giant magneto-resistive ratio (GMR) circuit board. The two circuit boards and battery are encased within the threaded steel insert using Stycast 1080 SI, an electronics potting epoxy. The antenna is a 0.76-mm thick copper-clad disk made of Duroid 6010 and is connected to the electronics via solder connections near the projectile axis. The rearward disk of copper cladding abuts the 1.52-mm thick Duroid 5880 radome cap. The radome is in direct contact with the propellant gases during launch and is meant to shield the instrumentation package from thermal and mechanical damage.
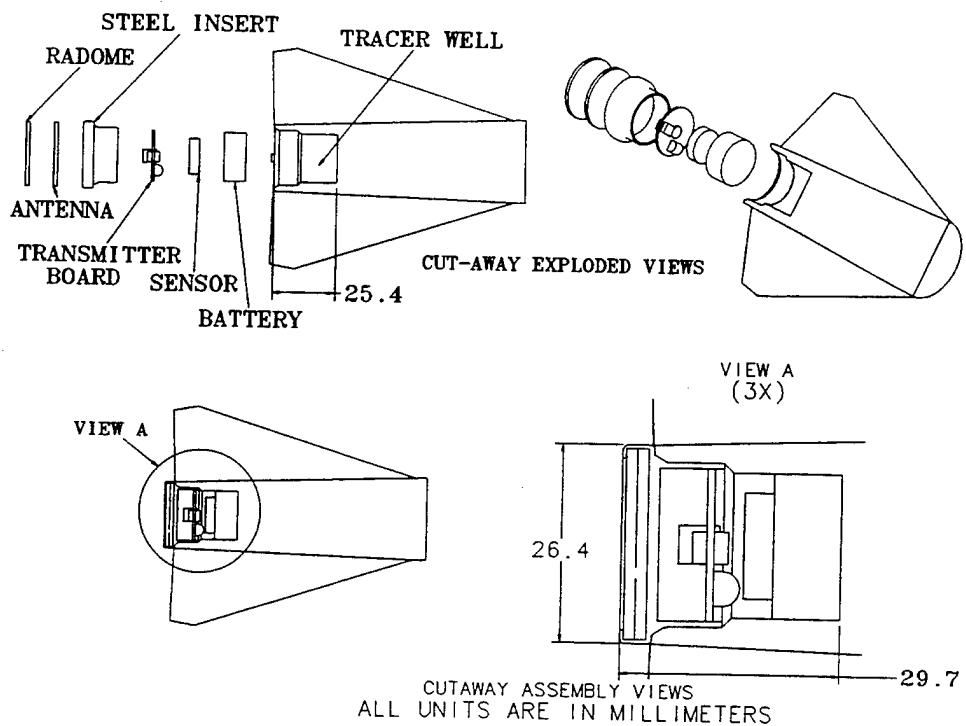
Figure 2. HSTSS Instrumentation Package.

The simplified HSTSS geometry used in the thermal analysis is shown in Figure 3. The fins are not included in the thermal analysis, as will be discussed, and are omitted from the figure. The individual electronic components, including circuit boards, battery, and solder connections, etc., are modeled as the Stycast 1080 SI in which they are encased. It is assumed that the HSTSS is a solid mass without air spaces, represented by seven single-material zones with a total of six materials.
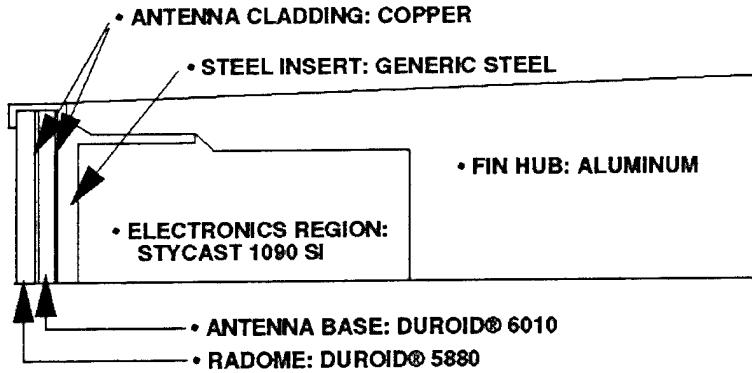
Figure 3. Simplified HSTSS Geometry Model.

Table 1 lists the HSTSS components and their physical and thermal properties of interest, all of which are assumed constant in the ensuing analysis. The critical temperature, T_{crit}, for each material is the melt temperature, except for the battery, in which case, the critical temperature is the estimated operational threshold temperature. The Duroid and Stycast materials have small conductivity and diffusivity compared to the metals and are expected be insulative. The radome has the additional characteristics of low melt temperature and large latent heat of melt, rendering it a prospective ablative shield. The solder used in the electronic connections is not modeled in the analysis, but its comparatively low melt temperature is a survivability criterion that must be considered. The aluminum oxide hard coat on the fin hub is excluded from the analysis and is omitted from the table.

Table 1. Physical and Thermal Properties of HSTSS Components

Component	Material	ρ (kg/m^3)	k (J/kg/K)	c_p (J/kg/K)	$\alpha(\frac{k}{\rho c_p})$ (m^2/K)	T_{crit} (K)	L (kJ/kg)
Fin Hub	Aluminum	2790	177.0	875	7.25×10^{-5}	933	Not used
Threaded Insert	Steel	7820	45.0	434	1.33×10^{-5}	1800	Not used
Potting	Stycast 1080 SI	700	0.19	1256	2.16×10^{-7}	380	Not used
Antenna	Copper	8930	401.0	385	1.17×10^{-4}	1358	Not used
Antenna Potting	Duroid 6010	2900	0.41	1000	4.04×10^{-7}	623	Not used
Radome	Duroid 5880	2200	0.26	960	3.38×10^{-7}	623	1.16×10^4
Battery	N/A	Not used	Not used	Not used	Not used	505	Not used
Solder	Lead & Tin	Not used	Not used	Not used	Not used	511	Not used

3. SURFACE HEAT TRANSFER MODELS

3.1 In-Bore Surface Heat Transfer

The in-bore projectile surface heat transfer characteristics were obtained from a separate analysis involving the interior ballistic code XKTC (Gough 1990) and the in-bore heat transfer code ARL XBR-2D (Conroy 1991; Crickenberger, Talley & Talley 1994). The XKTC code models a transient multiple phase reacting flow field with convective ignition to produce interior ballistic parameters of gas and propellant state and velocity, propellant position, as well as projectile motion. Usually, the spatially and temporally varying core flow parameters of gas pressure, temperature, and velocity from XKTC are used as input to the XBR-2D code to compute gun tube wall temperature profiles. In order to compute the conditions on the fin hub surface, a transformation from Eulerian to Lagrangian coordinate systems was implemented. The projectile fin was then treated as an immobile surface and the gun tube wall treated as a moving surface. The XKTC computation required approximately 30 seconds on a Silicon Graphics Inc. (SGI) Challenge computer using a single R8000 processor. The XBR-2D computation required approximately 1 second on the same computer. These times reflect the computer usage for the simulation of the in-bore portion of the event only.

The in-bore surface heat transfer characteristics were generated for the U.S. Army M865 projectile. The results were adapted for use in the present study, considering that the HATR uses the same cartridge and class of propellant as the M865. Figure 4 shows the computed
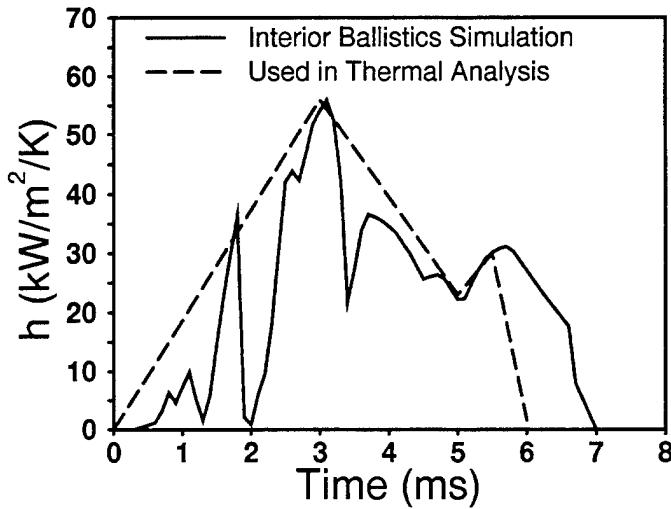
Figure 4. In-Bore Surface Heat Transfer Coefficient History.

heat transfer coefficient, h, acting on the fin hub. The original computational result consists of heat transfer coefficient histories at several locations on the fin hub, and the history shown in Figure 4 is representative of the overall behavior. The heat transfer coefficient undergoes several large fluctuations, with the maximum value of 55 kW/m^2/K reached about 3 ms into the event. Figure 4 also shows a piecewise distribution that was constructed and used in the ensuing heat conduction analysis. This was done as a quick, conservative, manual implementation of the heat conduction modeling software, although the original history could have been implemented in a more precise fashion. In addition, the distribution used in the thermal analysis was prescribed to decrease approximately 1 to 1.5 ms earlier than that of the interior ballistics analysis to account for the reduction in in-bore time.

Figure 5 shows the computed in-bore gas temperature, T_g, acting on the fin hub. The gas temperature experiences a sudden rise to a maximum of about 3300 K after propellant ignition, then slowly declines to a value of about 2400 K at 7 ms into the event. As was the case with the heat transfer coefficient, a quick, conservative, manual implementation of the gas temperature history was used. As shown in the figure, a constant value of 3400 K was used in the present thermal analysis.
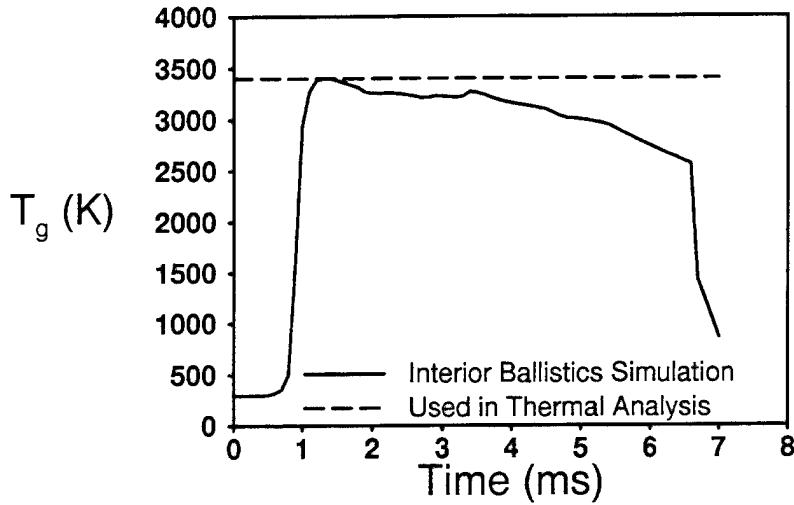
Figure 5. In-Bore Gas Temperature History.

The heat transfer coefficient and gas temperature histories are used in the present analysis to generate the local instantaneous heat transfer rate per unit area, q, from

$$q = h(T_{aw} - T_{wall}) \tag{1}$$

in which T_{wall} is the local instantaneous wall temperature and T_{aw} is the adiabatic wall temperature, assumed to be equal to T_g.

6

3.2 In-Flight Surface Heat Transfer

The in-flight (i.e., aerodynamic) heat transfer coefficient distributions were obtained from a separate analysis involving a three-dimensional (3-D) parabolized Navier-Stokes (PNS) computational fluid dynamics code. The PNS code models turbulent, viscous, steady, supersonic attached flow over the projectile using a space-marching finite difference technique. The numerical solution is advanced downstream by numerically integrating in the main flow direction, requiring about 1 central processing unit (CPU) hour on a Cray Y-MP computer per solution for this class of finned configurations. The PNS technique, because it is space marching, is significantly more computationally efficient than time-marching techniques. The PNS approach has been used extensively in house to study the aerodynamics and heat transfer characteristics of large caliber finned KE projectiles. Details of the technique and an informative synopsis of its application to fin-stabilized KE projectiles are presented by Guidos and Weinacht (1993).

The in-flight heat transfer rates are obtained from steady state flow solutions generated using the PNS numerical method. The computations are performed by specifying a constant wall temperature boundary condition, yielding a distribution of surface heat transfer rate. The in-flight heat transfer coefficient used in the present thermal analysis was adapted from computations for the M735 and M829 projectiles (Guidos & Weinacht 1993). Those results showed that the in-flight heat transfer coefficients on the cylinder portion of the fin hub are similar for the two projectiles and only slightly dependent on velocity in the speed regime of interest here. The in-flight heat transfer coefficient distribution on the cylinder portion of the M829 projectile at a velocity of 1670 m/s, from Guidos and Weinacht (1993), is depicted in Figure 6. Using this figure as a guide, a value for h of 1600 W/m^2/K was selected as the aerodynamic heat transfer coefficient to apply on the fin hub surface, excluding the base. An upper boundary on h, the value was held constant with respect to time in the present analysis.

The adiabatic wall temperature distributions were obtained by prescribing a free-stream temperature recovery factor, r_f, consistent with turbulent boundary layer flow, i.e.,

$$T_{aw} = T_\infty (1 + r_f \frac{(\gamma - 1)}{2} M_\infty^2)$$ (2)

in which T_∞ is the free-stream temperature, M_∞ is the free-stream Mach number, γ is the ratio of specific heats (taken to be 1.4). A value of 0.9 was used for r_f. Equation (2) yields values of T_{aw} of 1289 K at the launch velocity and 920 K at 3-km range for the HATR projectile. A linear variation with respect to time was assumed in the heat conduction computations. The values of T_{aw} provided by Equation (2) have been shown to

7

be comparable to those of the PNS technique everywhere except near the fin leading edges for this class of problem (Guidos & Weinacht 1993).

Equation (1) is then used during the heat conduction analysis to extract the instantaneous heat transfer rate from h, T_{aw}, and T_{wall}. The exception is the in-flight surface heat transfer condition for the projectile base, which is prescribed to be adiabatic after the projectile exits the gun tube.
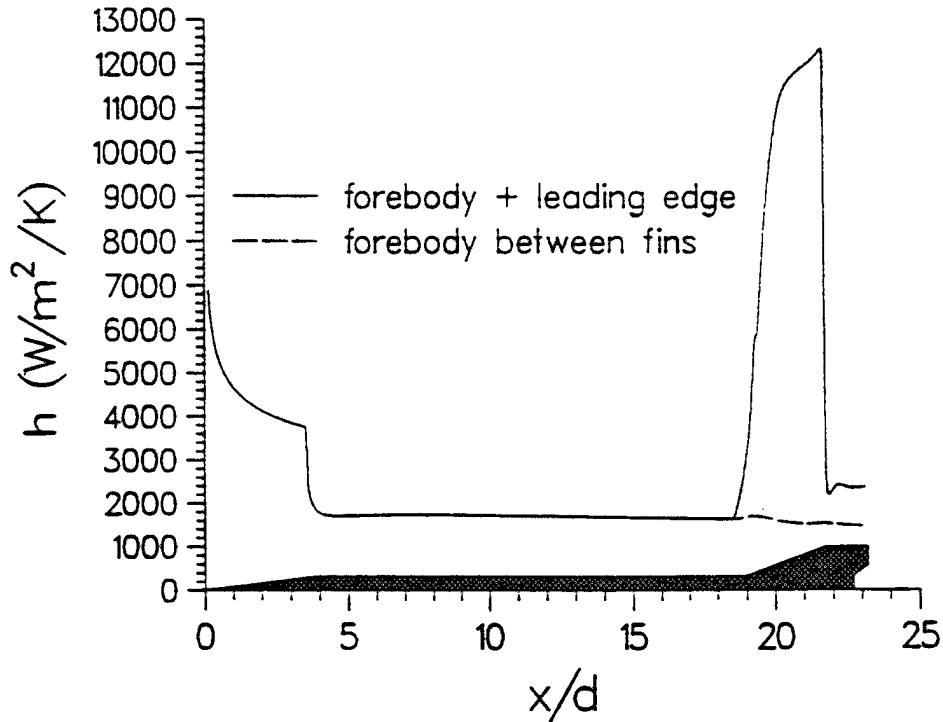
Figure 6. Aerodynamic Surface Heat Transfer Coefficient, M829 Projectile, V=1670 m/s.

4. IN-DEPTH THERMAL RESPONSE MODELS

4.1 2-D Numerical Model of Multiple Material HSTSS

A 2-D analysis was conducted for the multiple material HSTSS configuration using Integrated Design and Analysis Software (IDEAS) developed by Structural Dynamics Research Corporation, Milford, OH. IDEAS uses a multiple material, multiple zone, finite volume formulation to model heat conduction within a generalized geometry. The 1-D numerical and analytical results for steel rod convective heating presented by Guidos (1995) were used to validate the IDEAS software before the HSTSS analysis. The computational time for the

8

HSTSS configuration was approximately 2 hours on an SGI Indigo 2 workstation using a single R4400 processor for the 3-second launch and flight event.

The simplified 2-D axisymmetric HSTSS configuration described earlier was used as a basis for constructing the computational grid, shown in Figure 7. The grid is unstructured, consisting of 7053 elements and 5093 nodes. Grid spacing at the projectile surface is approximately 0.14 mm. The full length of the fin hub is not modeled; rather, only the rearmost 55 mm are included in the grid. This forward-most boundary is prescribed to be held at a constant temperature of 298 K. The initial temperature throughout the model is prescribed to be 298 K.
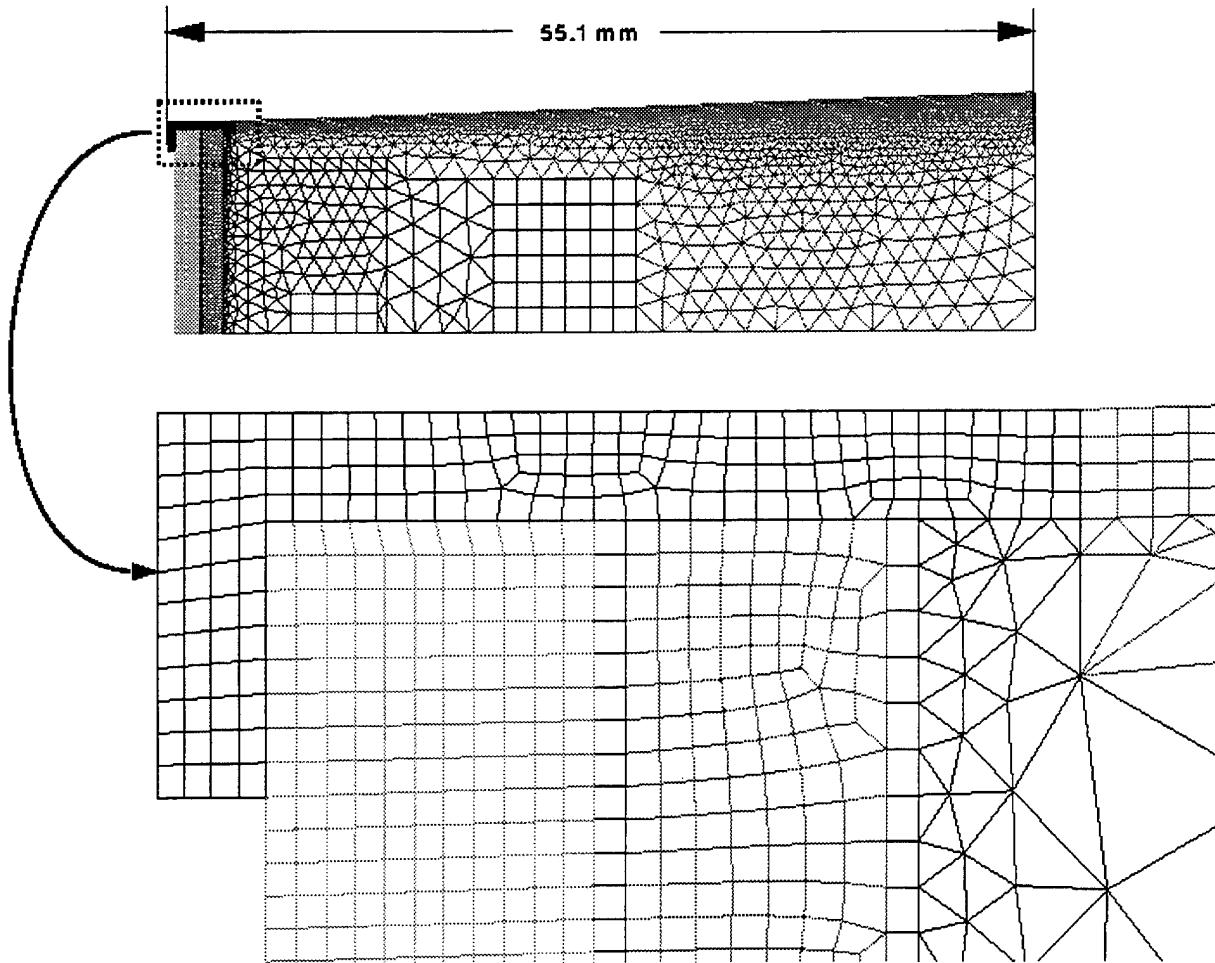
Figure 7. 2-D Axisymmetric Grid.

4.2 1-D Numerical Model of Radome

A 1-D numerical approach is useful for determining the thermal response of the radome because the surface grid spacing and resulting computer time required to resolve the thermal gradients are substantially more demanding than elsewhere in the fin hub. As will be shown, the 1-D numerical analysis shows that the radome surface melts during the in-bore launch phase, requiring a surface melt boundary condition not available in the version of IDEAS used here.

The 1-D numerical heat conduction analysis was performed in the present study using a single material code described by Dwyer (1990); Sturek, Dwyer, and Ferry (1990); and Yam (1991). The scheme is a time-accurate, iterative, implicit, finite volume technique cast in time-varying generalized coordinates. For this study, a 2-D version of the code with a surface melt condition was used in a 1-D mode. The code had been previously validated by comparing to 1-D analytical results for steel rod convective heating with no melting (Guidos 1995) and 1-D numerical results for M256 gun tube heating and melting (Weinacht and Conroy 1996).

Melting is modeled in the 1-D code by assuming that the melted material and heat contained within are transported away adiabatically. The ablative boundary conditions, implemented when the surface temperature reaches the melt temperature, are the same as those presented in Weinacht and Conroy (1996), i.e.,

$$T_{wall} = T_{melt} \tag{3}$$

$$\rho L \frac{ds}{dt} = h(T_{aw} - T_{wall}) - k\frac{dT}{dy} \tag{4}$$

in which the surface temperature, T_{wall}, is set equal to the melt temperature, T_{melt}. The density is ρ, the latent heat of melt is L, the surface regression rate is ds/dt, and the temperature gradient at the surface is dT/dy. The complete system of equations is solved iteratively at each time step because the regression rate is an additional unknown.

The 1-D numerical result was generated assuming a 2-mm thick radome and using 100 grid points. The minimum grid spacing required at the surface to resolve the temperature gradient was 0.05 micrometer, much smaller than the 0.14-mm spacing used in the 2-D numerical analysis. The 1-D numerical simulation was performed using the same heat transfer coefficient and adiabatic wall temperature histories as the 2-D results above. The simulation was performed for the in-bore part of the event and required approximately 1 hour of CPU time on an SGI Challenge computer using a single R8000 processor.

4.3 1-D Analytical Model of Radome

A simple 1-D analytical model was formulated to perform an additional calculation of radome surface melting. It is assumed that the amount of heat conducted into the material is small compared to the amount of heat lost because of surface melting. As in the 1-D numerical approach discussed before, it is also assumed that the melted material and the heat contained within are transported away adiabatically. The resulting heat balance equation is

$$\rho L \frac{ds}{dt} = h(T_{aw} - T_{melt}) - \rho c_p (T_{melt} - T_i) \frac{ds}{dt} \tag{5}$$

in which the initial temperature is T_i. Equation (5) can be re-arranged to solve for the melt depth, δ, i.e.,

$$\delta = s|_{t_f} - s|_{t_i} = \int_{t_i}^{t_f} \frac{h(T_{aw} - T_{melt})}{\rho[L + c_p(T_{melt} - T_i)]} dt \tag{6}$$

which can be solved analytically or integrated numerically, depending on the complexity of h and T_{aw} as functions of t.

5. RESULTS

Temperature contours from the 2-D axisymmetric model are shown in Figure 8 at times of 1, 2, and 3 seconds, respectively. The contours show that heat reaching the interior of the HSTSS is transported primarily from the outer fin hub rather through than the base. In this respect, the Duroids and Stycast appear to be effective heat insulators, although the radome thermal response is examined in more detail subsequently. The electronics region is minimally affected by the heat input throughout the 3-second event, except near its outer edge. The heat conducted from the outer fin hub through the rearward copper cladding of the antenna is likely over-predicted because the computational model is constructed with both copper disks in direct contact with the steel insert. In the actual configuration, the rearward copper cladding and the steel insert are separated by 3 mm of Duroid 6010.

Figure 9 shows locations of four temperature monitor points used here to summarize the critical thermal response of the HSTSS. The fin hub surface monitor point is located 18 mm from the base. The battery monitor point is located 21 mm from the projectile base and 2 mm from the outer edge of the electronics region. The antenna monitor point is located on the rearward copper antenna disk, on the projectile axis, near the solder connections. The radome surface monitor point is also located on the axis, focusing attention on the ablation process that is anticipated during launch.
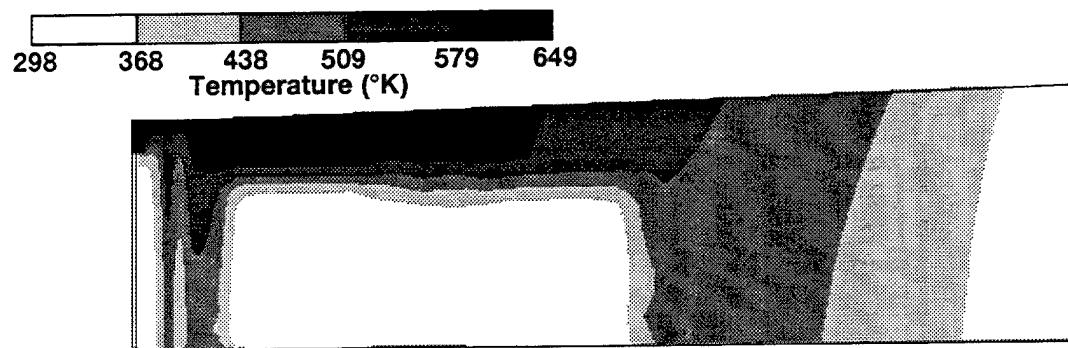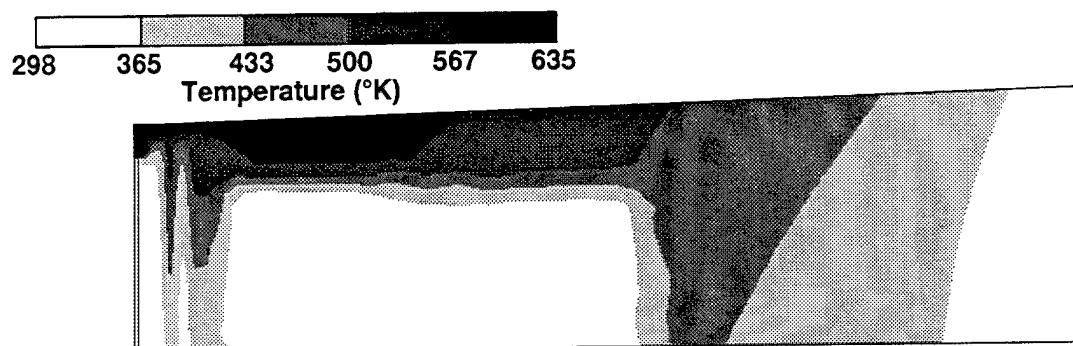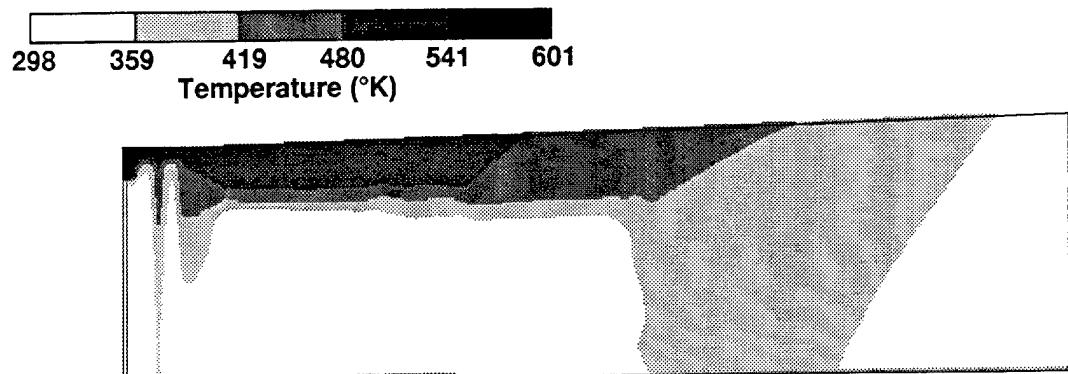
Figure 8. Computed Temperature Contours at 1, 2, and 3 seconds.
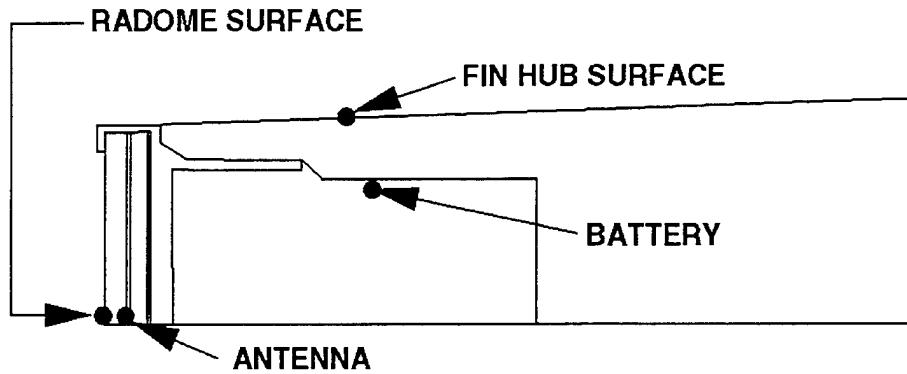
Figure 9. Temperature Monitoring Points.

The computed thermal response at the fin hub surface monitor point is shown in Figure 10. The 2-D axisymmetric result shows the maximum in-bore temperature at the fin hub surface monitor point to be approximately 565 K. Upon gun tube exit, the temperature is predicted to fall to approximately 375 K. The in-flight temperature is predicted to increase monotonically to approximately 620 K at 3-seconds into flight.
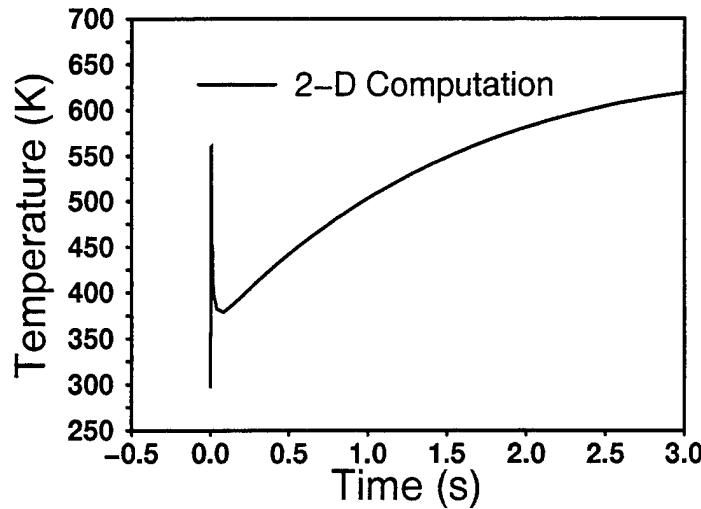
Figure 10. Computed Temperature Response at Fin Hub Surface Monitor Point.

The computed thermal response at the battery monitor point is shown in Figure 11. The 2-D axisymmetric result shows that the battery is far enough removed from the effects of massive in-bore heating that no abrupt temperature increase occurs. At approximately 400 ms, the temperature begins to noticeably increase to a value of 340 K at 3 seconds into flight. This is safely below the lead/tin solder melt temperature and the battery operational threshold temperature, but only 40 K below the Stycast 1080 SI potting melt temperature. Depending upon the precise thermal response at the outer edge of the electronics section, some local melting of the potting could occur, although late enough into the 3-second flight as to not be a concern.
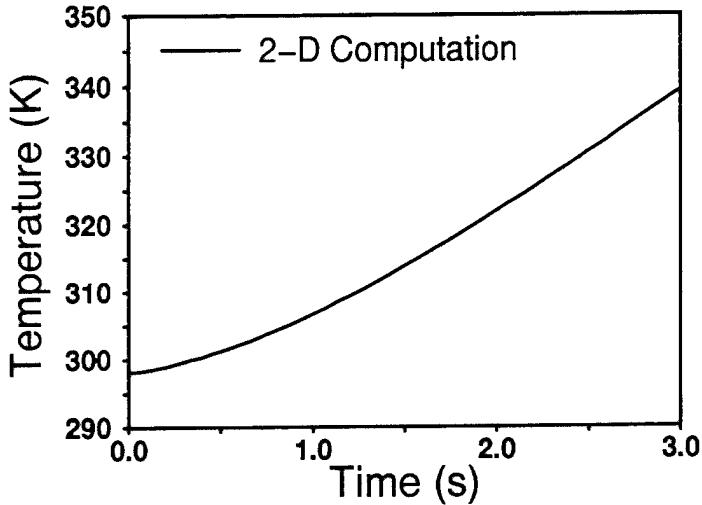
Figure 11. Computed Temperature Response at Battery Monitor Point.

The computed thermal response at the antenna monitor location is shown in Figure 12. As was the case with the battery monitor point, the 2-D axisymmetric result shows that the antenna is far enough removed from the effects of massive in-bore heating that no abrupt temperature increase occurs. At approximately 200 ms, the temperature begins to increase steadily to a value of 460 K at 3 seconds into flight. This is below the Duroid 5880, copper, and lead/tin solder melt temperatures. The antenna thermal response was shown in the contour plots to be determined by the heat conducted through the steel insert rather than through the radome.

14
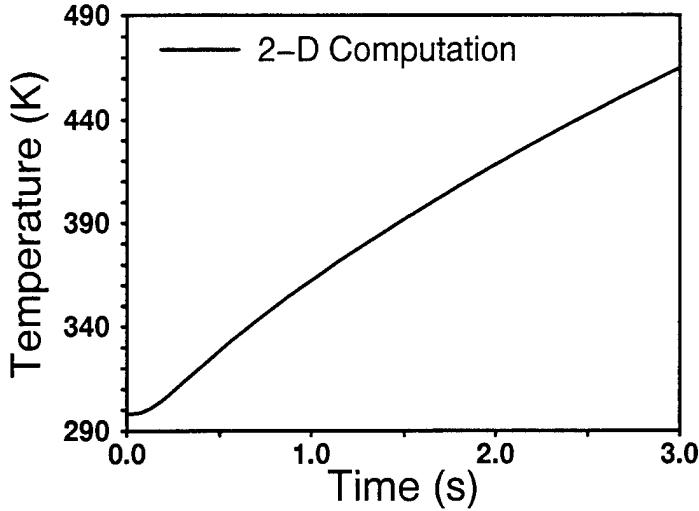
Figure 12. Computed Temperature Response at Antenna Monitor Point.

The 2-D axisymmetric model showed the radome surface temperature to rapidly increase above the Duroid 5880 melt temperature while still in bore. It also showed that no heat was transported through the radome to the antenna. However, a closer examination of the 2-D result revealed that the grid spacing was inadequate to resolve the large thermal gradient beneath the radome surface. A more detailed analysis was performed on the radome using the 1-D numerical approach with a surface melt condition.

Figure 13 shows the computed in-bore thermal response of the radome surface monitor point using the 1-D numerical model. As already mentioned, the 1-D result employs grid spacing small enough to resolve the large temperature gradient near the radome surface. The 1-D result shows that the surface temperature abruptly increases to the melting temperature of 623 K within 1 ms and that melting occurs for approximately 5 ms.

Figure 14 shows the computed temperature distribution within the radome at different in-bore times using the 1-D numerical model. When the temperature gradient is largest, the thermal layer is less than 10 μm thick. As the projectile exits the gun tube, the maximum temperature is 450 K and the thermal layer is less than 30 μm thick. After the projectile exits the gun tube, an adiabatic surface heating condition is assumed to exist on the radome surface, effectively halting heat flow into the radome. The thermal layer within the radome is orders of magnitude thinner than the radome itself. It may be concluded that the thermal energy contained in the radome is insufficient to affect the antenna.

15
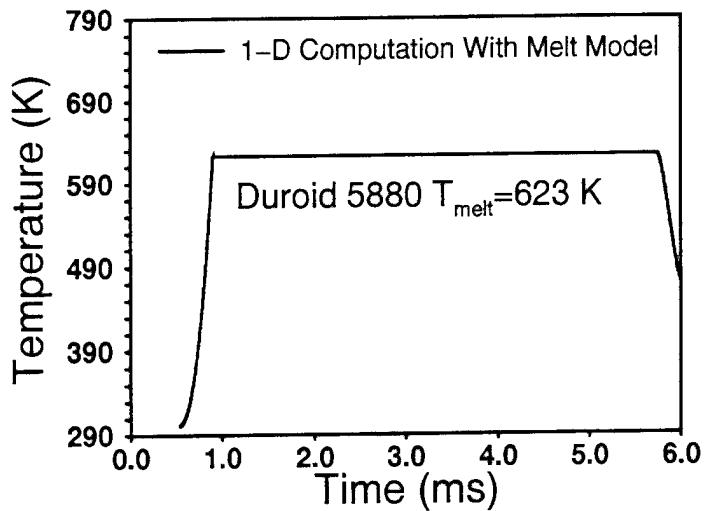
Figure 13. Computed Temperature Response at Radome Surface Monitor Point.
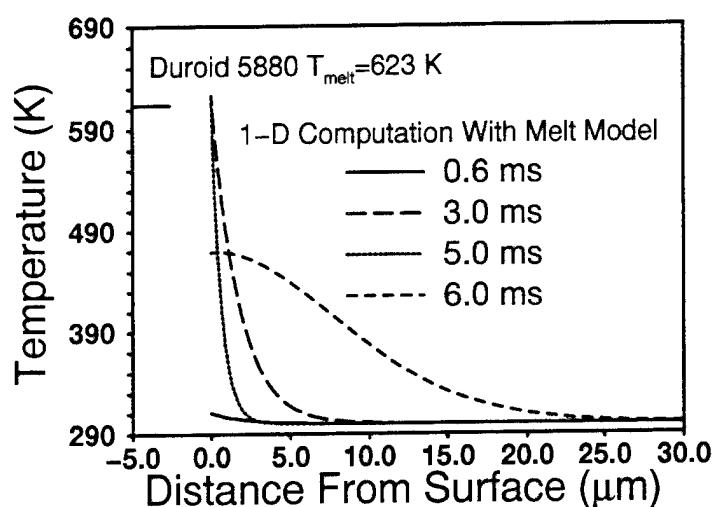
Figure 14. Computed Temperature Distribution in Radome.

16

The result shows that the Duroid 5880 radome is an effective ablative insulator in this case. Despite the fact that the 2-D model does not contain adequate grid resolution or a melting condition, it correctly portrays the fact that no heat is conducted through the radome to the antenna. If the melt depth of the radome were of no interest, an adiabatic boundary condition on the radome surface would suffice for predicting the thermal response of the HSTSS interior components.

Figure 15 shows the predicted in-bore melt depth of the radome as a function of time for both the 1-D numerical and 1-D analytical models. The methods agree to within 3% at 5.5 ms into the event and show the in-bore melt depth of the radome to be approximately 0.55 mm, less than the 1.52-mm total radome thickness.
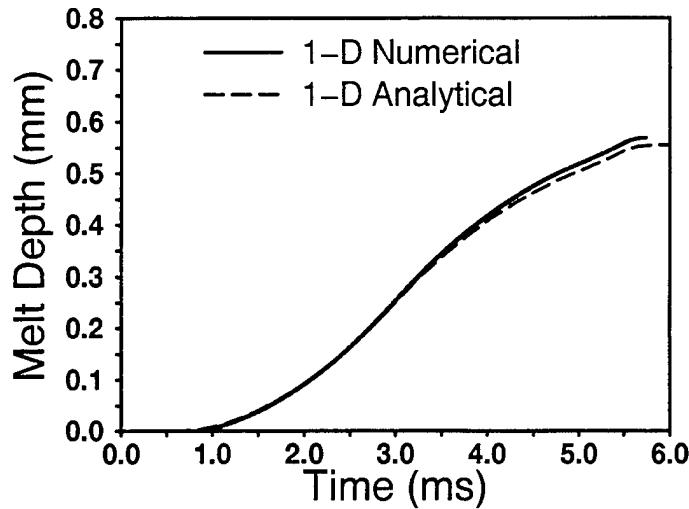
Figure 15. Computed Radome Melt Depth.

Figure 15 also demonstrates the usefulness of the 1-D analytical approach for estimating the melt depth for this radome material during large-caliber launch conditions. The assumption that the amount of heat conducted into the material is small compared to the amount of heat lost because of surface melting appears to be valid here. The 1-D analytical model provides a fast engineering approach for tailoring the radome thickness at gun tube exit and thereby influencing the in-flight dielectric properties of the radome, an important consideration for optimum antenna functionality.

6. CONCLUSION

A computational thermal analysis has been presented for an HSTSS mounted in the tracer well of a large caliber KE projectile. The in-bore surface heat transfer model was taken from results of a numerical interior ballistics study. The in-flight surface heat transfer model was taken from the results of a numerical aerodynamics study. The transient thermal response within the projectile fin hub and HSTSS was computed using three approaches: a 2-D axisymmetric numerical model, a 1-D numerical model, and a 1-D analytical model. Thermal survivability criteria were compiled and applied to the results to characterize the thermal viability of the current design.

The electronics region is predicted to reach temperatures that are below the melt temperatures of the potting and the solder connections, as well below the operational temperature threshold of the battery. The outer edge of the potting is predicted to reach temperatures only 40 K below its melt temperature late into the flight and could experience some local melting, depending on the precise thermal response. The antenna is predicted to reach temperatures below the melt temperatures of the Duroid 6010, copper, and the solder connections. The radome is predicted to reach its melt temperature within 1 ms of the 5.5 ms in-bore event, but the total ablation depth of 0.5 mm is less than the 1.52-mm total radome thickness. The radome serves as an effective insulator, as the ablation process removes heat from the system that could otherwise be transported to the antenna.

The use of the 2-D multiple material heat conduction model, along with the 1-D numerical and analytical models that include a surface melt condition, provides a fast computational pre-test design methodology. In addition, the 1-D analytical prediction for radome melt depth is shown to agree with the 1-D numerical prediction to within 3% at gun tube exit. The 1-D analytical model provides a fast engineering approach for tailoring the radome thickness at the gun tube exit and thereby influences the in-flight dielectric properties of the radome, an important consideration for optimum antenna functionality. At the time of this writing, no test projectiles had yet been fired. The thermal analysis herein suggests that the present HSTSS design will survive the in-bore and in-flight environments associated with a large-caliber gun system without experiencing catastrophic thermal failure.

7. REFERENCES

Burdeshaw, M. R., and W.H. Clay, "Subminiature Telemetry Tests Using Direct Fire Projectiles," BRL-MR-3893, U.S. Army Ballistic Research Laboratory, Aberdeen Proving Ground, Maryland, February 1991. (AD B236899)

Conroy, P., "Gun Tube Heating," BRL-TR-3300, U.S. Army Ballistic Research Laboratory, Aberdeen Proving Ground, Maryland, December 1991. (AD A243265)

Crickenberger, A.B., R.L. Talley, and J.Q. Talley, "Modifications to the XBR-2D Heat Conduction Code," ARL-CR-126, U.S. Army Ballistic Research Laboratory, Aberdeen Proving Ground, Maryland, April 1994. (AD A279330)

D'Amico, W.P., L.W. Burke, R.J. Faulstich, and A. Hooper, "The Hardened Subminiature Telemetry and Sensor Technology Demonstration Phase," ARL-TR-1206, U.S. Army Research Laboratory, Aberdeen Proving Ground, Maryland, October 1996. (AD A317178)

Davis, B.S., "Microelectromechanical Accelerometer Shock Testing and Assessment for Use as a Part of a Projectile Inertial Measurement Unit," ARL-MR-287, U.S. Army Research Laboratory, Aberdeen Proving Ground, Maryland, February 1996. (AD B203966)

Davis, B.S., "Flight Test Results of HSTSS Low Cost Spin and Drag Sensors," ARL-MR-335, U.S. Army Research Laboratory, Aberdeen Proving Ground, Maryland, August 1996. (AD B215590)

Dwyer, H., "Calculation of Low Mach Number Reacting Flows," AIAA Journal, Vol. 28, No. 1, pp. 98-105, January 1990.

Gough, P.S., "The XNOVAKTC Code," BRL-CR-627, U.S. Army Ballistic Research Laboratory, Aberdeen Proving Ground, Maryland, February 1990. (AD A220153)

Guidos, B.J., "Computed In-Flight Temperature Response of a 120-mm XM797 Gas Generator Training Round Nose Cap," ARL-MR-267, U.S. Army Research Laboratory, Aberdeen Proving Ground, Maryland, October 1995. (AD302378)

Guidos, B., and P. Weinacht, "Parabolized Navier-Stokes Computation of Surface Heat Transfer Characteristics for Supersonic and Hypersonic KE Projectiles," ARL-TR-191, U.S. Army Research Laboratory, Aberdeen Proving Ground, Maryland, August 1993. (AD A268858)

Sturek, W., H. Dwyer, and E. Ferry, Jr., "Prediction of In-Bore and Aerodynamic Heating of KE Projectile Fins," U.S. Army Ballistic Research Laboratory, Aberdeen Proving Ground, Maryland, BRL-MR-3852, August 1990. (AD A226402)

Weinacht, P., and P. Conroy, "A Numerical Method for Predicting Thermal Erosion in Gun Tubes," ARL-TR-1156, U.S. Army Research Laboratory, Aberdeen Proving Ground, Maryland, July 1996. (AD A311443)

Yam, C., "An Investigation of Flow Structure and Heat Transfer Characteristics of Three Dimensional Flows," PhD Dissertation in Mechanical Engineering, University of California at Davis, California, 1991.

INTENTIONALLY LEFT BLANK.

LIST OF SYMBOLS

c_p	specific heat
d	reference diameter
h	heat transfer coefficient
	temperature
k	thermal conductivity
L	latent heat of melt
M	Mach number
q	heat transfer rate per unit area
r_f	free-stream temperature recovery factor
s	surface location in fixed coordinate system perpendicular to surface
T	temperature
t	time
V	projectile velocity
x, y	spatial coordinates

Greek Symbols

δ	surface melt depth
γ	ratio of specific heats
ρ	density

Subscripts

aw	adiabatic wall condition
$crit$	critical condition
f	final condition
g	gas condition
i	initial condition
$melt$	melt condition
$wall$	wall condition
∞	free-stream condition

INTENTIONALLY LEFT BLANK.

NO. OF COPIES	ORGANIZATION
2	ADMINISTRATOR DEFENSE TECHNICAL INFO CENTER ATTN DTIC DDA 8725 JOHN J KINGMAN RD STE 0944 FT BELVOIR VA 22060-6218
1	DIRECTOR US ARMY RESEARCH LABORATORY ATTN AMSRL CS AL TA RECORDS MANAGEMENT 2800 POWDER MILL RD ADELPHI MD 20783-1197
1	DIRECTOR US ARMY RESEARCH LABORATORY ATTN AMSRL CI LL TECHNICAL LIBRARY 2800 POWDER MILL RD ADELPHI MD 207830-1197
1	DIRECTOR US ARMY RESEARCH LABORATORY ATTN AMSRL CS AL TP TECH PUBLISHING BRANCH 2800 POWDER MILL RD ADELPHI MD 20783-1197
1	HQDA DAMO FDQ DENNIS SCHMIDT 400 ARMY PENTAGON WASHINGTON DC 20310-0460
1	CECOM SP & TRRSTRL COMMCTN DIV AMSEL RD ST MC M H SOICHER FT MONMOUTH NJ 07703-5203
1	PRIN DPTY FOR TCHNLGY HQ US ARMY MATCOM AMCDCG T M FISETTE 5001 EISENHOWER AVE ALEXANDRTA VA 22333-0001
1	PRIN DPTY FOR ACQUSTN HQ US ARMY MATCOM AMCDCG A D ADAMS 5001 EISENHOWER AVE ALEXANDRIA VA 22333-0001

NO. OF COPIES	ORGANIZATION
1	DPTY CG FOR RDE HQ US ARMY MATCOM AMCRD BG BEAUCHAMP 5001 EISENHOWER AVE ALEXANDRIA VA 22333-0001
1	DPTY ASSIST SCY FOR R&T SARD TT T KILLION TFE PENTAGON WASHINGTON DC 20310-0103
1	OSD OUSD(A&T)/ODDDR&E(R) J LUPO TFE PENTAGON WASHINGTON DC 20301-7100
1	INST FOR ADVNCD TCHNLGY THE UNIV OF TEXAS AT AUSTIN PO BOX 202797 AUSTIN TX 78720-2797
1	DUSD SPACE IE765 J G MCNEFF 3900 DEFENSE PENTAGON WASHINGTON DC 20301-3900
1	USAASA MOAS AI W PARRON 9325 GUNSTON RD STE N319 FT BELVOIR VA 22060-5582
1	CECOM PM GPS COL S YOUNG FT MONMOUTH NJ 07703
1	GPS JOINT PROG OFC DIR COL J CLAY 2435 VELA WAY STE 1613 LOS ANGELES AFB CA 90245-5500
1	ELECTRONIC SYS DIV DIR CECOM RDEC J NIEMELA FT MONMOUTH NJ 07703

3	DARPA
	  L STOTTS
	  J PENNELLA
	  B KASPAR
	3701 N FAIRFAX DR
	ARLINGTON VA 22203-1714

NO. OF COPIES	ORGANIZATION	NO. OF COPIES	ORGANIZATION

1 SPCL ASST TO WING CMNDR
50SW/CCX
CAPT P H BERNSTEIN
300 O'MALLEY AVE STE 20
FALCON AFB CO 80912-3020

1 USAF SMC/CED
DMA/JPO   M ISON
2435 VELA WAY STE 1613
LOS ANGELES AFB CA 90245-5500

1 US MILITARY ACADEMY
MATH SCI CTR OF EXCELLENCE
DEPT OF MATHEMATICAL SCI
MDN A MAJ DON ENGEN
THAYER FIALL
WEST POINT NY 10996-1786

1 COMMANDER
US ARMY YUMA PROVING GRND
ATTN STEYT MT EA   C HASTON
YUMA AZ 85365-9110

3 COMMANDER
US ARMY YUMA PROVING GRND
ATTN STEYT MT AT A   A HOOPER
YUMA AZ 85365-9110

3 COMMANDER
US ARMY YUMA PROVING GRND
ATTN STEYP RS EL   R FAULSTICH
YUMA AZ 85365-9110

1 COMMANDER
US ARMY WSMR
ATTN STEWS ID   JESSE NUNEZ
BLDG 1506
WSMR NM 88002

2 COMMANDER
US ARMY MICOM
ATTN AMSMI RD   W WALKER
AMSMI SW   AL FROELICH
REDSTONE ARSENAL AL 35898-5222

1 DIRECTOR
US ARMY REDSTONE
TECH TEST CTR
ATTN STERT TE F TD   R EPPS
REDSTONE ARSENAL AL 35898-8052

1 DIRECTOR
USARL
ATTN AMSRL EP ED   R ZETO
FT MONMOUTH NJ 07703-5601

4 COMMANDER
US ARMY ARDEC
ATTN AMSTA AR AET A   K KENDL
M AMORUSO   J MENDEZ
R KINASEWITZ
PICATINNY ARSENAL NJ 07806-5000

1 COMMANDER
US ARMY ARDEC
ATTN AMSTA AR AEC T   SAL LONGO
PICATINNY ARSENAL NJ 07806-5000

1 COMMANDER
US ARMY DUGWAY PROV GRND
ATTN TECH LIB
DUGWAY UT 84022

3 COMMANDER
US ARMY ARDEC
ATTN AMSTA FSP A   F SCERBO
R SICIGNANO   S SARULLO
PICATINNY ARSENAL NJ 07806-5000

1 COMMANDER
US ARMY RSRCH OFC
ATTN AMXRO RT IP TECH LIB
PO BOX 12211
RESEARCH TRIANGLE PARK NC
27709-2211

1 DIRECTOR
US ARMY STRICOM
ATTN AMCPM ITTS IMO
VICTOR KREPACKI
12350 RESEARCH PKWY
ORLANDO FL 32826-3276

1 ARPA/ESTO
ATTN K GABRIEL
3701 N FAIRFAX DR
ARLINGTON VA 22203-1714

4 COMMANDER NSWC
ATTN TECH LIB
J ELLIOTT CODE G61
D HAGAN CODE G304
J FRAYSSE G33
17320 DALGREN RD
DAHLGREN VA 22448-5000

1 COMMANDER NSWC
ATTN TECH LIB
SILVER SPRING MD 20903-5000

NO. OF COPIES	ORGANIZATION	NO. OF COPIES	ORGANIZATION
1	COMMANDER NSWC ATTN TECH LIB CHINA LAKE CA 93555-6001	1	COMMANDER USAF WRIGHT LABORATORY ATTN WL MNMF MR DICK MABRY 101 WEST EGLIN BLVD EGLIN AFB FL 32542-6810
1	COMMANDER NAWC WEAPONS DIV CODE 54AOOOD C3904 ATTN DON SCOFELD 1 ADMINISTRATION CIR CHINA LAKE CA 93555-6001	1	CDR USAF ARNOLD ENGRNG DVLPMENT CTR ATTN ILT DREW WALTON APLD TCHNLGY DIV 1099 AVE C ARNOLD AFB TN 37389-9011
1	COMMANDER NAWC WEAPONS DIV CODE 54A000D ATTN SHERRI GATTIS 1 ADMINISTRATION CIR CHINA LAKE CA 93555-6001	1	UNIV OF MARYLAND DEPT OF AEROSPACE ENGRG ATTN J ANDERSON COLLEGE PARK MD 20742
1	COMMANDING OFFICER USMC AVIATION DETACHMENT ATTN COL MOYER 1 ADMINISTRATION CIR CHINA LAKE CA 93555-6001	1	NEW MEXICO STATE UNIV PHYSICAL SCIENCE LAB ATTN WADE CRADDOCK BOX 3002 LAS CRUCES NM 88003-0002
1	OFFICER IN CHARGE NAVAL EOD FACILITY ATTN TECH LIB INDIAN HEAD MD 20640	1	UC BERKELEY DEPT OF EECS ATTN R HOWE 231 CORY HALL 1770 BERKELEY CA 94720-1770
1	PM NAVAL SURF FIRE SUP NAVAL SEA SYSTEMS CMD ATTN CODE PMS429 CPT DENNIS MORRAL 2531 JEFFERSON DAVIS HWY ARLINGTON VA 22202	1	BSAC/UC BERKELEY ELECTRONICS RES LAB DEPT OF EECS ATTN A PISANO BERKELEY CA 94720
1	COMMANDER NUWC ATTN CODE 8322 DR KURT W ROTH BLDG 1246 NEWPORT RI 0284	1	ANALOG DEVICES ATTN D WHITLEY J DOUSCHER J SCARSI 831 WOBURN ST WILMINGTON MA 01887-3462
1	COMMANDER USAF DVLPMNT TEST CTR ATTN AFDTC DRI MR THOMAS A SIPOS 101 WEST D AVE STE 117 EGLIN AFB FL 32542-5495	2	SENSOR APPLICATIONS ATTN D GOODMAN M CLYMER 23 INDUSTRIAL DR WATERFORD CT 06385
1	COMMANDER USAF WRIGHT LABORATORY ATTN WL MNAV MR JERRY WICHENBACH 101 WEST EGLIN BLVD EGLIN AFB FL 32542-6810	2	MICRO CRAFT AEDC OPNS TECH & ANALYSIS BR ATTN J SHAVER G WALKER AEDC TN 37389

NO. OF COPIES	ORGANIZATION
1	WADDAN SYSTEMS ATTN M SINGH 25429 RYE CANYON RD VALENCIA CA 91355
1	ROCKWELL INTL CORP AUTONETIC ELEC SYS DIV ATTN R CHRISTIANSEN 3370 MIRALOMA AVE PO BOX 3105 ANAHEIM CA 92803-3105
2	THE CHARLES STARK DRAPER LAB INC ATTN J ELWELL J SITOMER 555 TECHNOLOGY SQ CAMBRIDGE MA 02139-3563
2	DYNAMIC SCIENCE INC ATTN S ZARDAS P NEWMAN PO BOX N ABERDEEN MD 21001
2	MOTOROLA SENSOR PRODUCTS DIV ATTN R FRANK D WALTERS PHOENIX AZ 85008
1	SILICON DESIGNS INC ATTN J COLE 1445 NW MALL ST ISSAQUAH WA 98027-5344
1	SYSTRON DONNER INERTIAL DIV ATTN B SAGE 2700 SYSTRON DR CONCORD CA 94518-1399
1	PROJECT MANAGER AYDIN VECTOR DIV ATTN F COOK 47 FRIENDS LANE NEWTON PA 18940
3	ULTRALIFE BATTERIES INC ATTN JOSEPH N BARRELLA DEAN LEVEY OLIVER GROSS 1350 ROUTE 88 SO PO BOX 622 NEWARK NY 14513

NO. OF COPIES	ORGANIZATION
1	ULTRALIFE BATTERIES INC 3799 BUCKINGHAM DR ATTN WAYNE BREM DOYLESTOWN PA 18901
1	MCC HIGH VALUE ELECTRONIC ATTN ROBERT F MIRACKY 3500 W BALCONES CTR DR AUSTIN TX 78759-5398
1	PICO SYSTEMS ATTN JEFFERY BANKER 329 NORTH 14TH ST TOLEDO OH 43624-1454
1	TEXAS INSTRUMENTS ATTN STEVEN C LAZAR MICROWAVE MIL COMPONENTS 13510 N CNTRL EXPRSWY 75243 PO BOX 655474 MS 402 DALLAS TX 76265
3	NATIONS INC ATTN CECIL BASSHAM JIM MOSLEY BOB CARPENTER 12249 SCIENCE DR STE 150 ORLANDO FL 32826-3276

ABERDEEN PROVING GROUND

NO. OF COPIES	ORGANIZATION
2	DIR ARL ATTN AMSRL CI LP TECH LIB BLDG 305

39	DIR USARL
	ATTN AMSRL WM IMAY
	      J ROCCHIO
	AMSRL WM W C MURPHY
	AMSRL WM WB F BRANDON
	      T BROWN L BURKE
	      W D'AMICO B DAVIS
	      E FERGUSON T HARKINS
	      D HEPNER M HOLLIS (5 CYS)
	      R MCGEE
	AMSRL WM WC T HAUG T VONG
	      J BORNSTEIN R VON WAHLDE
	AMSRL WM WD A NIILER
	AMSRL WM WE J LACETERA
	AMSRL WM WF W DOUSA
	      S FORTIER G MORLEY
	      J WALL
	AMSRL WM P A HORST

NO. OF
COPIES   ORGANIZATION

AMSRL WM PB   P PLOSTINS
        D LYON   B GUIDOS (5 CYS)
        P WEINACHT   H EDGE
        M BUNDY   J SAHU
        K FANSLER
AMSRL WM PA   G KELLER
        P CONROY

3   CDR USATECOM
        ATTN AMSTE TC
        AMSTE CT T   J SCHNELL
        AMSTE CT M   M JOINER

2   CDR USAATC
        ATTN STEAC TE   H CUNNINGHAM

NO. OF
COPIES   ORGANIZATION

   2   ULTRALIFE BATTERIES (UK) LTD
          ATTN DR COLIN NEWNHAM
                NEIL SCHOLEY
          18 NUFFIELD WAY
          ABINGDON
          OXFORDSHIRE OX 141TG
          ENGLAND

REPORT DOCUMENTATION PAGE

Public reporting burden for this collection of information is estimated to average 1 hour per response, including the time for reviewing instructions, searching existing data sources, gathering and maintaining the data needed, and completing and reviewing the collection of information. Send comments regarding this burden estimate or any other aspect of this collection of information, including suggestions for reducing this burden, to Washington Headquarters Services, Directorate for Information Operations and Reports, 1215 Jefferson Davis Highway, Suite 1204, Arlington, VA 22202-4302, and to the Office of Management and Budget, Paperwork Reduction Project (0704-0188), Washington, DC 20503.

1. AGENCY USE ONLY (Leave blank)	2. REPORT DATE August 1997	3. REPORT TYPE AND DATES COVERED Final

4. TITLE AND SUBTITLE

Thermal Analysis of a Subminiature Telemetry Sensor Mounted in a Kinetic Energy Projectile Base

5. FUNDING NUMBERS

PR: W0027883K1

6. AUTHOR(S)

Hollis, M.S.L.; Guidos, B.J.; Conroy, P.J. (all ARL)

7. PERFORMING ORGANIZATION NAME(S) AND ADDRESS(ES)

U.S. Army Research Laboratory
Weapons & Materials Research Directorate
Aberdeen Proving Ground, MD 21010-5066

8. PERFORMING ORGANIZATION REPORT NUMBER

9. SPONSORING/MONITORING AGENCY NAME(S) AND ADDRESS(ES)

U.S. Army Research Laboratory
Weapons & Materials Research Directorate
Aberdeen Proving Ground, MD 21010-5066

10. SPONSORING/MONITORING AGENCY REPORT NUMBER

ARL-TR-1425

11. SUPPLEMENTARY NOTES

12a. DISTRIBUTION/AVAILABILITY STATEMENT

Approved for public release; distribution is unlimited.

12b. DISTRIBUTION CODE

13. ABSTRACT (Maximum 200 words)

A computational thermal analysis is presented for a hardened subminiature telemetry sensor system (HSTSS) mounted in the tracer well of a large caliber fin-stabilized kinetic energy projectile. The HSTSS discussed here is designed to provide a record of roll history. The in-bore and in-flight projectile surface heat transfer conditions are adapted from two previous studies in numerical interior ballistic and computational aerodynamics. The combined heat transfer model is used in the present study to provide boundary conditions for computations of surface and in-depth transient thermal response of the HSTSS components. A two-dimensional axisymmetric multiple material numerical approach is used to model the HSTSS and projectile base over the complete in-bore and in-flight event. A one-dimensional numerical approach with a surface melt condition is used to model the protective plastic radome on the HSTSS while in bore. A one-dimensional analytical approach for high-speed melting is presented and compared to the numerical model. The analysis allows a pre-test evaluation to be made of the thermal integrity of the HSTSS design for a large caliber launch and flight environment.

14. SUBJECT TERMS

aerodynamic heating, munitions, telemetry subminiature sensor, heat conduction, supersonic flow

15. NUMBER OF PAGES

37

16. PRICE CODE

17. SECURITY CLASSIFICATION OF REPORT Unclassified	18. SECURITY CLASSIFICATION OF THIS PAGE Unclassified	19. SECURITY CLASSIFICATION OF ABSTRACT Unclassified	20. LIMITATION OF ABSTRACT

NSN 7540-01-280-5500

Standard Form 298 (Rev. 2-89)
Prescribed by ANSI Std. Z39-18
298-102